Interaction of Scanning Probes with Semiconductor Nanocrystals; Physical Mechanism and Basis for Near-Field Optical Imaging†

Yuval Ebenstein, Eyal Yoskovitz, Ronny Costi, Assaf Aharoni, and Uri Banin*

Institute of Chemistry, the Farkas Center for Light Induced Processes, and the Center for Nanoscience and Nanotechnology, The Hebrew University of Jerusalem, Jerusalem 91904, Israel

Received: October 28, 2005; In Final Form: April 17, 2006

We investigate the modification of photoluminescence (PL) from single semiconductor nanocrystal quantum dots (NCs) in the proximity of metal and semiconducting atomic force microscope (AFM) tips. The presence of the tip alters the radiative decay rate of an emitter via interference and opens efficient nonradiative decay channels via energy transfer to the tip material. These effects cause quenching (or enhancement) of the emitter's PL intensity as a function of its distance from the interacting tip. We take advantage of this highly distance-dependent effect to realize a contrast mechanism for high-resolution optical imaging. AFM tips are optimized as energy acceptors by chemical functionalization with InAs NCs to achieve optical resolution down to 30 nm. The presented experimental scheme offers high-resolution optical information while maintaining the benefits of traditional AFM imaging. We directly measure the PL intensity of single NCs as a function of the tip distance. Our results are in good agreement with calculations made by a classical theoretical model describing an oscillating dipole interacting with a planar mirror.

Introduction

The presence of a dielectric tip causes strong modification of photoluminescence (PL) properties from nearby fluorophores.[1,2] This effect has been exploited to generate contrast for apertureless near-field scanning microscopy (A-NSOM) schemes.[3−5] Near-field microscopy provides enhanced resolution beyond the diffraction limit of far-field microscopy. In conventional NSOM,[6] light is driven through a subwavelength aperture and, practically, the resolution is limited by the size of the aperture and the optical skin depth of the metal coating, typically on the order of 100 nm.[7] In apertureless near-field microscopy, the resolution is obtained by perturbation of the optical field by a nanometer-sized tip in the proximity of the sample and resolution down to 1 nm was claimed.[8] Previous works measuring PL with A-NSOM reported a variety of optical phenomena such as PL enhancement and PL quenching. Various lateral PL distribution patterns were observed for seemingly similar experiments in which the PL of emitting specimens was measured with respect to a scanning tip position. Some of these effects have been explained by differences in experimental conditions such as the mode of excitation, tip treatment, and sample properties.[9] Recently, finite difference time domain simulations of such dipole−tip systems demonstrated that probe geometry has a substantial effect on the distance dependence of the interaction, shedding light on some of the observed PL patterns.[10] Here we investigate systematically the effect of PL quenching by AFM tips of different materials including tips coated by semiconductor nanocrystals (NCs).[11] We use an experimental scheme enabling simultaneous acquisition of AFM and apertureless near-field optical images while recording the distance-dependent behavior of the tip−sample system. The availability of these data for each point of the image provides insight into the nature of the tip-induced optical interaction with clear relevance to high-resolution microscopy schemes.

With the rapid progress of nanoscience and related technologies, efforts are made to enhance the available tool box for the study of nano systems and larger complex systems where nanoscale detail is required. The combination of AFM and high-resolution optical data measured simultaneously presents a powerful approach in this context.[12,13] Tapping-mode AFM (TAFM) is the technique of choice for the study of weakly bound nanostructures and soft biological samples because it does not inflict lateral forces on the sample. In this case, however, the optical interaction is averaged out due to the tip−sample distance modulations and specific experimental schemes are required to extract meaningful optical information.[14,15] Recently, Gerton et al. presented a method utilizing TAFM in which fluorescence photons are collected with respect to the tip position.[14] A similar scheme, but using standard time-correlated single-photon counting (TCSPC) hardware, is utilized in this study allowing extraction of distance-dependent optical data. We applied this distance-correlated single-photon counting (DCSPC) method to the investigation of semiconductor NCs that possess both measurable topography and fluorescence tunable by size, composition, and shape. In previous work, we already pointed out the potential use of NC-functionalized tips for a microscopy scheme based on fluorescence resonant-energy transfer (FRET).[11] Such tips are used here, and their optical interaction with the sample is characterized.

The obtained distance-dependent optical data provides insight into the interaction mechanisms of the fluorophore with the tip material and can be understood within the framework of fluorophores in front of a dielectric mirror. The radiative and nonradiative decay rates of an excited dipole fluorescing proximal to a metal film have been investigated extensively, both theoretically and experimentally.[16−20] The best agreement between experiment and theory was achieved by Chance, Prock, and Silbey (CPS) who calculated the total energy flux through

† Part of the "Chava Lifshitz Memorial Issue".

* Corresponding author. E-mail: Uri.Banin@huji.ac.il.

10.1021/jp056229o CCC: $33.50
Published on Web 05/26/2006

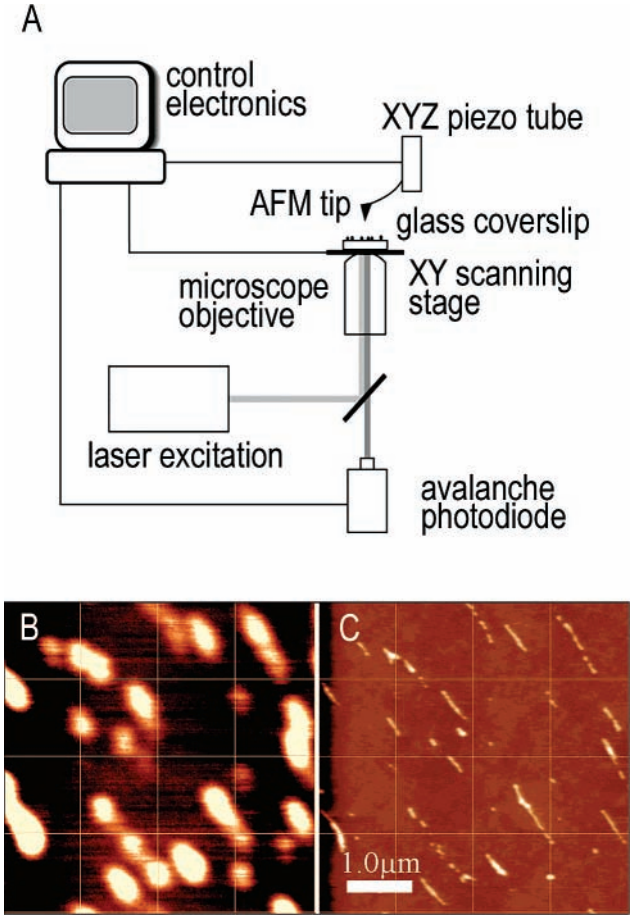

Figure 1. Schematic representation of the experimental setup. B and C are, respectively, correlated fluorescence and topography images of NC strings on glass, demonstrating the high degree of correlation between the two channels.

infinite planes above and below the dipole.[17] This method yields separate expressions for the radiative and nonradiative decay rates, thus enabling the formulation of expressions both for the lifetime and for the luminescence efficiency of the dipole as a function of its distance from an interface. The lifetime of emitting molecules and NC ensembles in front of a dielectric interface has been reported previously.[16,17,19−22]

More recently, the lifetime and intensity of single molecules and NCs in proximity to an AFM tip have been investigated.[5,14,23,24] These measurements have shown both quenching and enhancement of the fluorescence intensity depending on experimental conditions. We present measurements of the distance-dependent PL intensity from single NCs and compare our results with the theoretical predictions for the quantum efficiency of a dipole in front of a mirror using the CPS theory. The strong modulation of PL intensity in the presence of the tip is exploited for optical imaging based on PL quenching and provides a basis for future high-resolution microscopy schemes.

Experimental Section

The experimental setup (Figure 1A) comprises an AFM head (Veeco, Bioscope) mounted on top of an inverted optical microscope (Zeiss, Axiovert 100) equipped with a piezoelectric scanning stage (Nanonics, Flatscan), enabling simultaneous acquisition of AFM and optical data.[12] An example for a correlated PL-topography measurement of NCs on glass is shown in Figure 1B. As an excitation source, the 514 nm line of an Ar-ion laser is passed through a single-mode fiber for spatial filtering and tuned to circular polarization. The beam is collimated onto the back aperture of an oil immersion, high numerical aperture (NA) objective (Zeiss, ×100, NA 1.4), and focused to a diffraction-limited spot on the sample. Fluorescence is collected by the same objective in an epi-illumination configuration and filtered from the excitation light by passing through a dichroic mirror and a 514 nm Raman-edge filter. The collected fluorescence is focused on to the active area of an avalanche photodiode (APD) (Perkin-Elmer, SPCM-ARQ 13). In a typical measurement, a dilute solution of colloidal NCs (CdSe/ZnS, core/shell dots and rods) is spin-cast on a clean glass coverslip. The sample is raster-scanned across the excitation spot until NC fluorescence is detected. The scan is then stopped with the NC parked within the excitation spot. At this point, the AFM tip is scanned over the particle, and fluorescence photons are collected pixel by pixel in correlation with the tip lateral position. As the tip approaches the NC, the fluorescence count rate is modified and optical contrast is created in the collected photon distribution map. A typical acquisition time of one frame is between 2 and 4 minutes, depending on scan speed and image size. (A schematic animation is presented in Supporting Information Flash movie 1.)

Earlier works[4,23] performed such experiments with a fixed tip−sample distance achieving optical contrast for single molecules. We also perform contact-mode experiments in the first part of this work. In the second part, we employ TAFM measurements where fluorescence photons are collected in respect to the tip position.[14] We use TAFM combined with time-correlated single-photon counting to obtain the distance dependence of the optical process during imaging. We use standard time-correlation hardware where the counter computer card is triggered by the tip oscillation. This distance-correlated single-photon counting scheme (DCSPC) allows us to optimize the optical contrast by choosing optical data acquired at specific tip−sample distance regions as indicated by the distance-dependence measurements.

Three types of AFM tips were investigated including bare Si tips, platinum-coated tips, and NC-functionalized tips.[11] NC-functionalized tips were prepared by coating the tips first with a layer of MPTMS (mercaptopropyl-trimethoxysilane) linker molecules followed by immersion in a nanocrystal solution.

Results and Discussion

Two sets of experiments are presented; the first was conducted in contact-mode AFM, and the second was conducted in our combined TAFM−DCSPC scheme. By monitoring the optical PL images of single emitting NCs, we compare the quenching properties of the three types of AFM tips mentioned above.

Fluorescence Quenching in Contact-Mode AFM. Figure 2 shows typical optical images of single CdSe/ZnS NCs acquired in contact mode. In this mode, the tip apex maintains physical contact with the sample surface, thus maximizing the optical interaction. Because the tip induces lateral forces during scanning, the NCs are embedded in a ∼10 nm polymethylmetacrylate (PMMA) film to prevent sweeping of the particles to the scan borders.[25] Figure 2A was recorded using a commercially available platinum-coated tip (Mikromasch, CSC12). A distinct dark spot is apparent in the image corresponding to the position of the embedded NC. The size of these dark spots is typically on the order of 140 nm fwhm, well below the diffraction limit and the size of our excitation spot, which is on the order of 350 nm fwhm. We note that similar quenching results in terms of quench size and magnitude were presented recently by Farahani et al. for aluminum-coated tips.[26] The

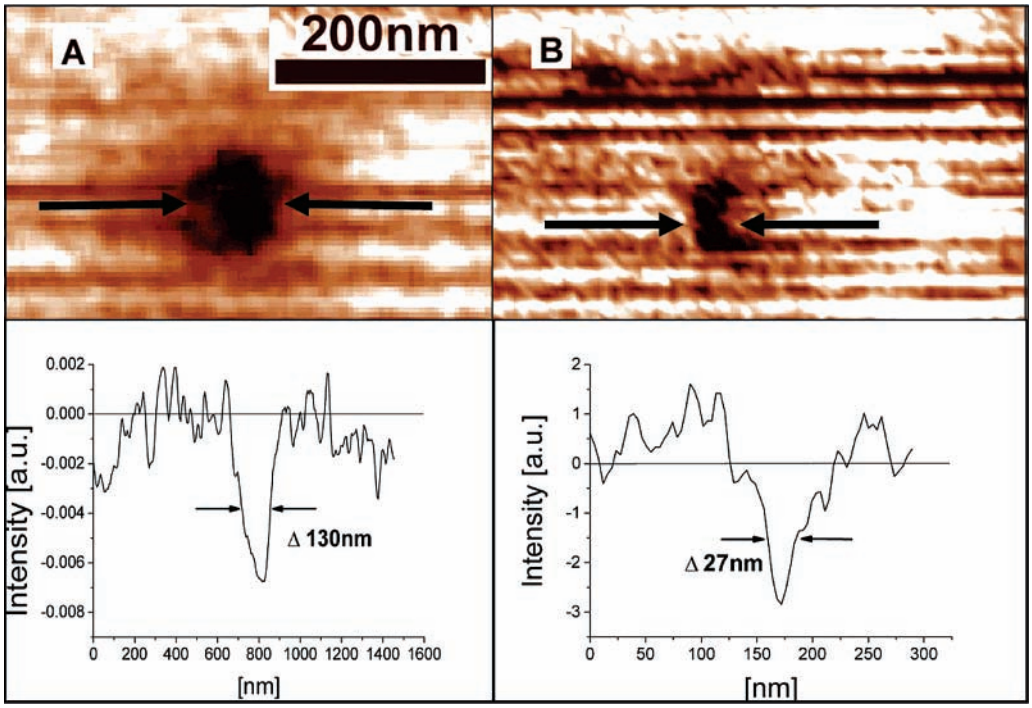

Figure 2. Quenching spots and corresponding fluorescence intensity cross sections of single NCs interacting with (A) a platinum-coated tip (130 nm fwhm) and (B) an InAs-functionalized tip (27 nm fwhm); the bottom shows the corresponding cross sections through the quenched spots along indicated arrows. The cross-section curve for the Pt tip (A) was smoothed by averaging over neighboring points. The cross section for the InAs-coated tip (B) was taken with a 3 pixel width profile line, and the curve was smoothed by averaging over neighboring points.

image in Figure 2B was recorded using a silicon tip (Mikromasch, CSC12) coated with a submonolayer of InAs NCs via chemical functionalization as described above.[11] These NCs were chosen because they are assumed to act as excellent energy acceptors for the CdSe/ZnS NCs in the sample. They possess a strong absorption cross-section at the region of interest, and emit weakly at ~1150 nm, outside our detection window (emission and absorption spectra for this NC configuration is shown in Supporting Information Figure S1). Using such functionalized probes resulted in quenched-fluorescence spots with diameters on the order of 30 nm fwhm, considerably smaller than those recorded with the metal-coated tips. We note that experiments executed with bare silicon tips did not result in tip-related optical contrast.

There are two possible explanations for the consistent difference in resolution between the metal-coated and NC-functionalized tips; first, the physical dimension of the interaction region of the tip is larger in the case of the metal-coated tip. Scanning electron microscope images of the two tip kinds show that there is indeed a difference in tip diameter between the two tips, as can be expected from the tip preparation process. Although both tips are based on a similar Silicon tip template, platinum-coated tips are significantly larger because of the evaporated metal film that is a few tens of nanometers thick. The other tip type is chemically coated with a submonolayer of NCs with a diameter of ~5 nm, keeping the sharpness of the original tip.

A second explanation for the improved resolution is related to the details of energy transfer processes between the NC fluorophore on the surface and the quenching tips. As discussed below, calculations of the characteristic energy-transfer distance for platinum versus InAs tip material could not explain the fivefold improvement in resolution for the InAs-functionalized tips. Furthermore, using the CPS model to describe both systems (solid and dashed lines in Figure 5B), we find that energy transfer actually occurs at shorter distance for the platinum case, which is in contradiction with our observations. A possible explanation for this discrepancy is that because the functionalized tip is composed of isolated NCs, we cannot assume it is well represented by the interaction of a chromophore donor with a planar acceptor surface described by the CPS theory (two-dimensional picture). A more appropriate picture for the NC-functionalized tips may be of an energy-transfer process between two point dipoles. Although the energy-transfer efficiency in the two-dimensional case has $1/d^3$ dependence on distance d, the dipole−dipole case takes the familiar Foerster form with $1/d^6$ distance dependence. This would lead to a steeper quenching profile and better resolution.

Fluorescence Quenching in Tapping-Mode AFM. As a consequence of the polymer embedding needed for contact-mode operation of the AFM, topography and other high-resolution information is not accessible in the former pictures. Furthermore, because the tip remains at a fixed distance from the emitting dipole, the detailed distance dependence of the interaction may not be studied. As mentioned earlier, tapping-mode AFM operation is desirable to provide topography as well as distance-dependent interactions.[14] To achieve this, we combine the AFM measurement with time-correlated single-photon counting (TCSPC). Briefly, an electrical trigger pulse is generated with each oscillation of the AFM tip and fed as a synchronization signal to a TCSPC computer card (Picoquant, Time Harp 200). The arrival time of each photon collected by the APD is recorded relative to the tip signal with 1 nsec resolution, and a histogram of photon arrival times is generated for each pixel in the image. Despite the high time resolution of our measurement, the acquired data files remain relatively compact because a time stamp is generated only for detected photons and histograming is performed on board and streamed to disk as a single histogram per pixel. This results in typical file sizes of about 256 MB for two 128 × 128 pixel^2 images (trace and retrace are acquired simultaneously), and these files can be displayed and analyzed on reasonably fast time scales. Because the frequency and

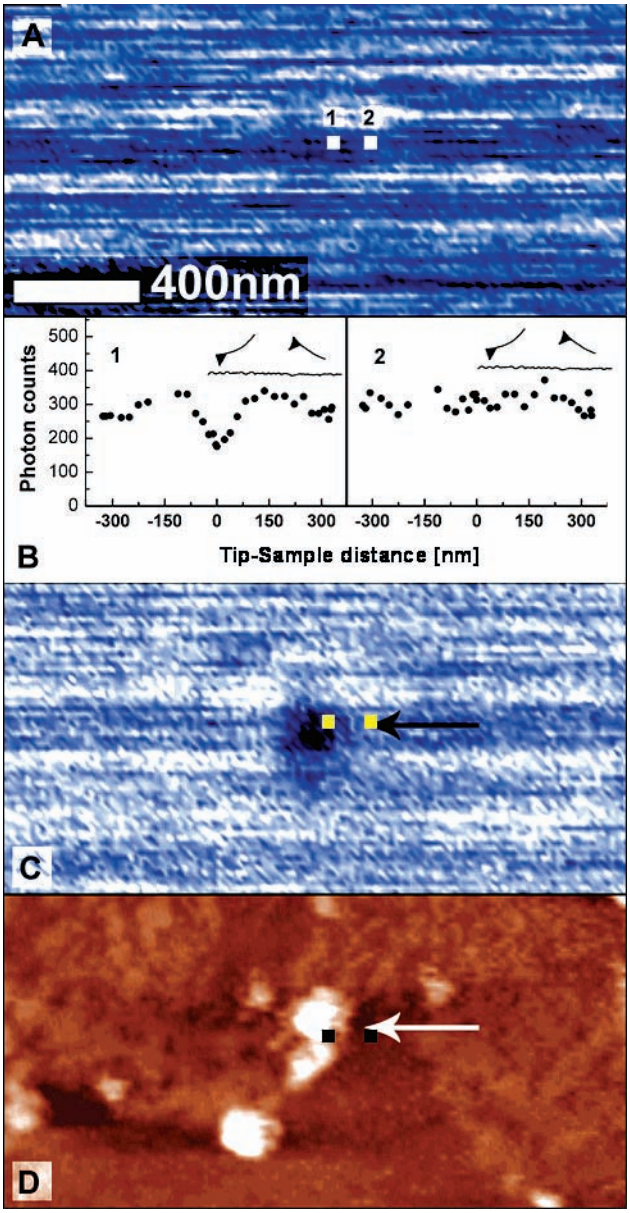

Figure 3. Signal-to-noise enhancement through generation of a distance-dependent fluorescence image. (A) Fluorescence image comprised of all of the collected photons. (B) Photon counts as a function of vertical tip−sample distance while tapping. The negative sign denotes tip motion toward the surface, and the positive sign denotes tip motion away from the surface. The two curves correspond to the two pixel positions designated as 1 and 2 in the optical image: (1) taken from an interaction region and showing distinct fluorescence quenching; (2) taken from a nearby area and showing no distance-dependent interaction with the sample. (C) Fluorescence image comprised of photons collected from the bottom 10 nm of the tip oscillation. (D) Simultaneously acquired AFM topography image of NCs on glass. Arrows mark the quenched particle. Pixel positions 1 and 2 are also marked on panels C and D: pixel 1 is clearly positioned on a particle, while pixel 2 is not.

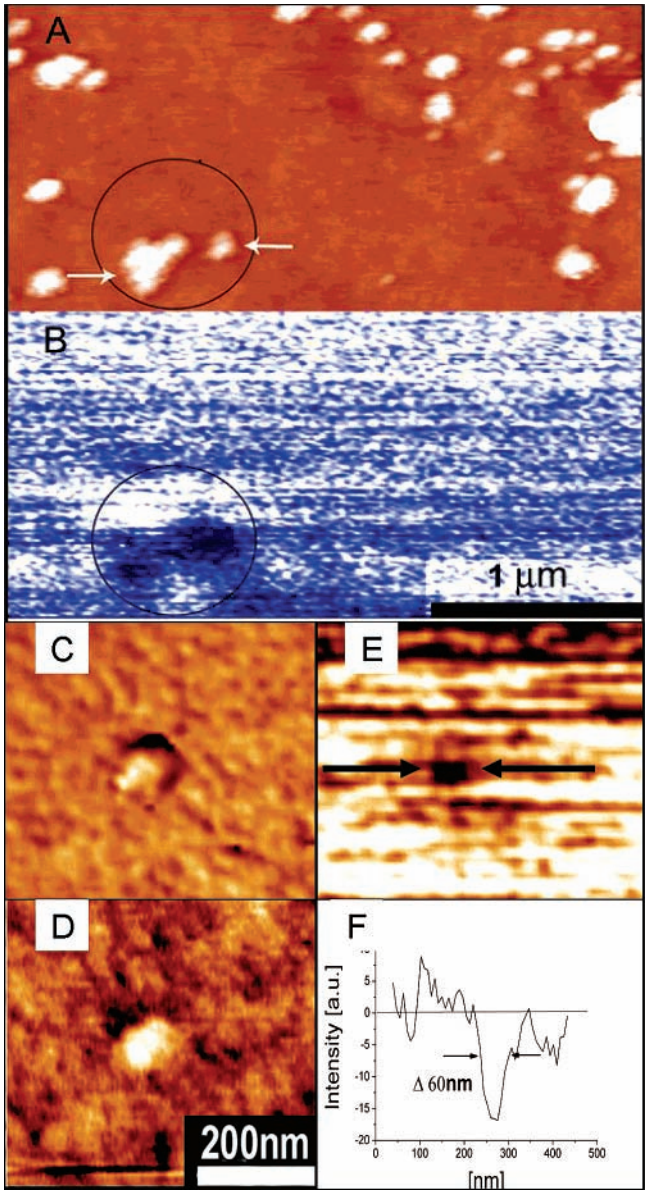

Figure 4. NCs on glass: topography (A) and distance-dependent fluorescence (B) images acquired with a platinum-coated tip. Two quenching spots optically distinguish between emitters in the far-field excitation region indicated by circles. C, D, and E are phase, topography, and fluorescence images, respectively, of a single NC acquired with an InAs-functionalized tip. As shown in the cross section of the fluorescence dark spot (F), the quenching spot in E has a diameter of ∼60 nm fwhm. The cross section was taken with a 3 pixel width profile line, and the curve was smoothed by averaging over neighboring points.

amplitude of oscillation are known, the histograms are easily converted to approach curves representing photon counts versus tip−sample vertical distance, yielding a distance-correlated single-photon counting scheme (DCSPC) with subnanometer precision.

Figure 3 shows a representative optical image using the DCSPC scheme. In the upper frame (Figure 3A), the far-field confocal image containing all of the photons recorded is presented. The NC jumps between high and low count-rate states, resulting in the visible streaks in the recorded optical image. This "blinking" phenomenon is typical of single NC emission.[27] The oscillation amplitude of the tip in this case (platinum-coated tip) is 350 nm, and no optical contrast can be resolved in the image because of the integration of the response at different tip−sample distances, which smears the effects recorded at very short distances. In Figure 3B, two approach curves of photon counts versus tip vertical position are presented corresponding to the two pixel positions designated 1 and 2 in the optical image. Curve 2 shows no distance-dependent characteristics, whereas curve 1 shows a systematic dependence of the photon counts on the tip−sample distance. The emission intensity is decreased as the tip approaches the NC. Because each photon is recorded with its respective tip position, it is now possible to generate an image composed of only the photons

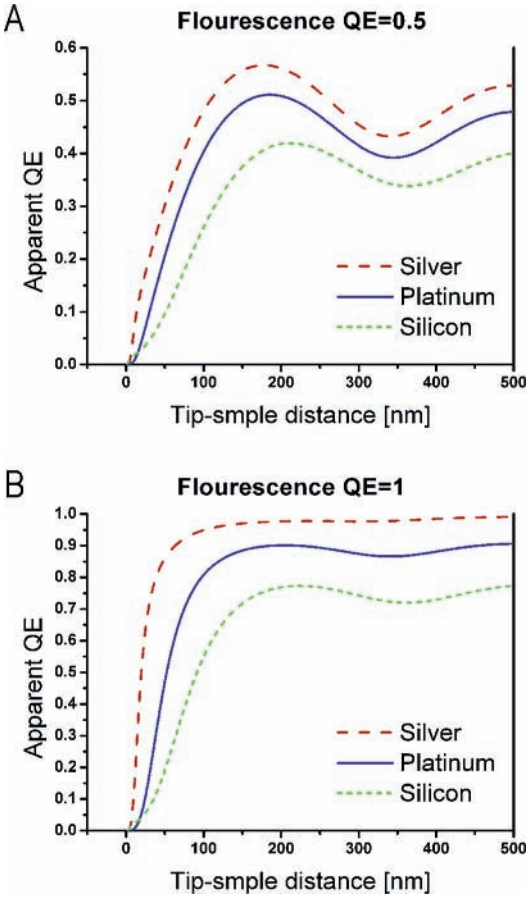

Figure 5. Calculated apparent quantum efficiency for a dipolar emitter with an unperturbed quantum efficiency of 0.5 (A) and 1 (B). The dipole is approached by a planar mirror of three different materials: silver (dashed line), platinum (solid line), and silicon (doted line). The calculated approach curve for InAs were found to be almost identical to that of silicon.

correlated to a desired range of tip−sample distances. The image in Figure 3C is composed of only the photons arriving while the tip was at the lowest 10 nm of its oscillation. A clear region of quenched fluorescence is revealed, demonstrating the enhancement of the signal-to-noise ratio relative to the unprocessed image. The simultaneously acquired topography image of NCs on glass is presented in Figure 3D. An arrow marks the particle under investigation. Pixels 1 and 2 are also marked on Figure 3C and D, showing that pixel 1 is positioned on a particle, whereas pixel 2 is not. Clearly, the acquisition of topography and other AFM data in conjunction with the optical information enables the assignment of optical data to specific regions of interest indicated by AFM. Although the far-field optical data gives chemical and other information common for fluorescence microscopy, the distance-dependent measurement offers the possibility of localizing the emitting species and gaining additional information from its distance-dependent behavior.

Two examples for the correlation between AFM and optical images are shown in Figure 4. In Figure 4A and B, the images were acquired by a platinum-coated tip. The topography image shows two NC aggregates within the excitation spot indicated by the circle. In a far-field image, the two aggregates would appear as a single fluorescence spot. Nevertheless, the two aggregates are clearly distinguishable in the quenching-induced optical image; moreover, the left quenching spot correlates to a specific region in the bigger of the two aggregates, indicating that it is composed only in part of emitting particles (marked with an arrow). Images obtained with a tip functionalized with InAs NCs are presented in the lower panels, Figure 4C, D, and E, corresponding to phase, height, and fluorescence images, respectively. Significantly improved optical resolution of 60 nm fwhm is achieved for a single NC (Figure 4E, cross section in Figure 4F). This resolution is similar to that of the correlated phase (Figure 4C) and topography (Figure 4D) scans. This improved resolution for InAs tips is consistent with our results in contact mode for the two tip types.

The images demonstrate the applicability of the method for optically resolving the location of fluorescent markers with high precision. This is especially attractive for biological samples such as DNA molecules and cells where physical structure may be determined by various AFM techniques while the optical data could also provide localized chemical information through the quenching of markers bound to the studied specimen.

An additional important feature of our experimental setup is the availability of both AFM and distance-dependent optical data for every pixel in the image. This enables the detailed analysis of approach curves correlated to specific locations in the topographic image. Specifically, we employ this to study the modification of PL intensity from single NCs interacting with the AFM tip. We focus on the investigation of energy transfer and quenching of PL by the approaching tip. We eliminate most enhancement effects by using in-plane polarized excitation, thus minimizing the coupling and concentration of the optical field at the tip apex. This is in contrast with the work of ref 14, which used perpendicular polarization and observed high-resolution enhancement effects used to image single nanocrystal fluorescence effectively. Nevertheless, because of the high NA of the microscope objective, a polarization component perpendicular to the sample plane also exists in our case. Farahani et al. in ref 26 use specially shaped optical antenna tips to achieve high-resolution enhancement effects as well, while regular tips coated with metal showed quenching.

Model Calculations of Distance-Dependent Fluorescence Quenching. The measurements are accompanied by theoretical analysis within the CPS framework. We model our system as a flat dielectric mirror (tip) approaching a single dipole (NC), fixed in vacuum (air) and parallel to the mirror. The total energy flux out of the upper and lower planes is calculated using the complex poynting vector and integrating its normal component over the plane.[28] Dividing the energy flux by the dipole energy gives the rate constant associated with energy loss through the plane. With these rate constants, we can now calculate the lifetime and quantum efficiency of the system for any given distance.[29] Using the CPS model, we calculate an apparent quantum efficiency (aQE), which is directly proportional to the PL intensity measured by integrating over all photons emitted to the half space below the dipole. We justify our choice of the parallel dipole model by the following: (1) the calculated aQE for a parallel dipole is much larger than that for the perpendicular one, making our measurement more sensitive to parallel dipole emission, and (2), the 2D degenerate nature of the NC emission dipole[30,31] ensures that there is always a parallel emission component to be detected.

Figure 5 shows the results of such calculations for various tip materials presenting the aQE versus tip−sample distance. At short ranges, most relevant to our present application, there is a steep reduction in aQE because of the efficient energy transfer to the tip. At longer distances, some oscillatory behavior is predicted because of the interference of the dipole with its image dipole in the dielectric material. Among the three calculated materials, silver shows a very steep response that could potentially translate into higher resolution. Practically,

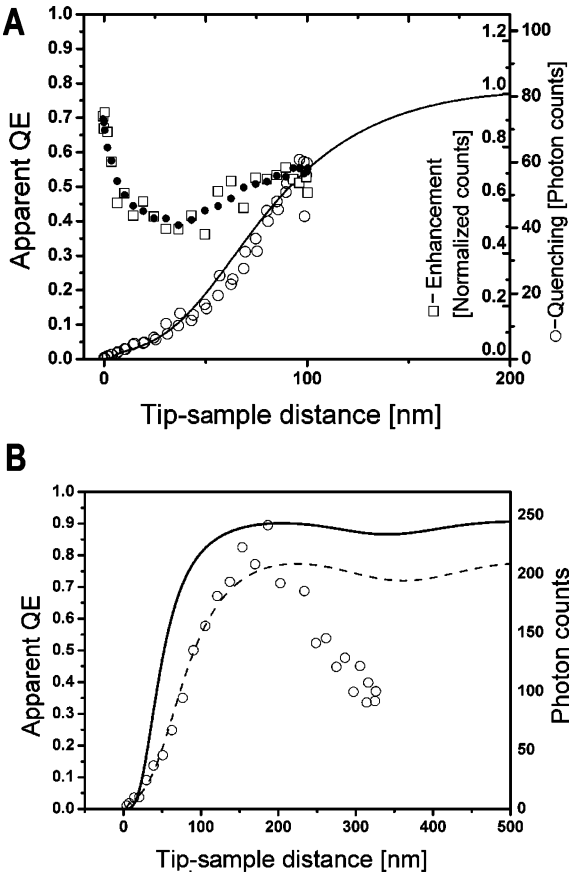

Figure 6. (A) Measured DCSPC traces with silicon tips and CPS model results. Open circles: measured photon counts vs distance showing quenching. Open squares: normalized average of five measurements showing enhancement. Black dots: four-point averaging of the enhancement data. In solid lines we plot the calculated apparent QE of a silicon mirror approaching an emitting dipole parallel to the surface. Good agreement to the measure data is observed. The dipole QE is assumed to be 1. (B) Measured photon counts of an NC as a function of the distance from a platinum-coated tip (open circles). We plot the calculated apparent QE of a platinum (solid line) and silicon (dashed line) mirror approaching an emitting dipole parallel to the surface. A better agreement to the silicon calculation up to 150 nm is observed. Beyond this distance, the reduction observed experimentally is not described by the model. (See text).

Ag is a problematic coating material for the tip because of its tendency for oxidation in ambient conditions. Another potential issue with silver is the possibility of enhanced emission via plasmonic effects, which are not treated here. An additional variable influencing the calculation is the unperturbed QE of the emitting dipole as can be seen comparing the distance dependence for QE = 0.5 (Figure 5A) with QE = 1 (Figure 5B). The effect of varying the dipole QE is manifested in the slope of the final 150 nm of the tip−sample approach curve. As nonradiative energy transfer becomes the dominant interaction mechanism, the slope becomes steeper for higher QEs.

In Figure 6, we present typical approach curves measured with silicon and platinum-coated tips approaching a NC with a 605 nm emission peak. All curves are measured during normal tapping-AFM operation with an average time of 5−10 ms per pixel to demonstrate the possibility for using this approach in practical imaging schemes with a frame time of a few minutes. For the approach curves presented here, we used a 2×2 pixel^2 binning, that is, 20−32 ms integration time per curve. By measuring the scattered excitation intensity as a function of tip distance, we derived a correction factor for the raw PL intensity data. This distance-dependent factor was used to correct the measured PL data for the change in excitation power due to backscattering of excitation photons from the tip. In addition, we plot the calculated apparent QE of an emitting dipole oriented parallel to the surface as it is approached by a planar silicon or platinum mirror. The theoretical curves use optical constants for the tip materials (Si, Pt, or InAs) taken from the literature.[32,33] The measured QE in solution for the NC sample was 0.5, and QE studies of single NCs support in this range a QE value of 1 for the emitting particles.[12,34] We therefore use a value of 1 for the unperturbed QE in the calculations as well.

In Figure 6A, we present the results for a silicon tip. Experimental and calculated DCSPC approach curves for InAs-functionalized tips were found to be almost identical to those of bare silicon and are therefore not presented. Although the CPS model is only a first approximation for the NC−tip system, experimental data (open circles) follows the theoretical curve (solid line) reasonably well for the 100 nm region measured. These efficient quenching properties are in contradiction with our observation of poor contrast in the silicon quenching images in comparison with the functionalized or metalized tips. Generating approach curves from nearby pixels in the Si case (open squares) reveals an additional effect of fluorescence enhancement by the proximity of the silicon tips. This enhancement effect for silicon tips has been reported previously[9,35] and exploited for high-resolution optical imaging.[14,33] We believe that this field enhancement by the sharp Si tip is caused by out-of-plane polarization components in the tightly focused excitation spot. The coexistence of both quenching and enhancement in our case results in low optical contrast for imaging with silicon tips, unlike platinum- and NC-coated tips, which give good contrast and present no enhancement effects in our experimental conditions. Using perpendicular polarization[14] or antenna-shaped tips[26] has given high-resolution fluorescence images of NCs.

It is possible that when the silicon tips are functionalized with InAs NCs, the latter serve to suppress the enhanced field at the tip apex in addition to their role as efficient energy acceptors for the studied sample PL. This twofold activity gives rise to the high quenching contrast visible in the images acquired with functionalized tips as opposed to bare silicon tips. In Figure 6B, an average of three approach curves from different particles measured with a platinum-coated tip (open circles) is plotted together with the calculated curves for platinum (solid line) and silicon (dashed line) mirrors. Here too, experimental data follows the silicon mirror model for the first 150 nm. The reason for the silicon-like behavior of the platinum-coated tip may lie in the fact that in our model we regard the tip as bulk platinum, neglecting the fact that it is composed of silicon coated by ∼30 nm of platinum with a titanium binding layer. Given the optical skin depth of platinum in this spectral region (few tens of nanometers),[36−38] it is possible that the silicon tip still has a significant effect on the quenching process. Furthermore, optical parameters for thin metal films depend strongly on film preparation and should be regarded with caution.[30]

Beyond 150 nm, we observe experimentally a decrease in count rates that deviates from the calculated behavior. To address this drop in photon count rate at longer tip−sample distances, we note another difference between our approximate model and the real system. It has been shown both experimentally and theoretically[21] that the emission pattern, that is, the spatial distribution of emitted photons from a dipolar emitter, is also strongly dependent on its distance from the interface. Although our model calculates the contribution of all photons emitted to the half space below it, in the experiment we are

restricted to collection from a finite solid angle determined by our microscope objective. A recent experiment by Buchler et al.,[39] featuring a scanning micro mirror−dye system and using a model containing variation in emission pattern, indeed showed strong intensity modulations even for a high QE emitter related to this effect.

Conclusions

We have demonstrated how tapping-mode AFM and fluorescence microscopy with distance-correlated single-photon counting may be combined to generate a wealth of information in a single correlated measurement. The combined tool used here offers the detailed structural characterization of AFM with the chemical information available by the optical microscope and the use of fluorescent tagging. In addition, the presence of the AFM tip enables both high-precision optical localization of emitting species and a detailed study of distance-dependent optical processes. Specifically, we have shown how energy transfer from emitting NCs to platinum-coated or NC-functionalized AFM tips results in quenching of PL in a distance-dependent manner. This process is appropriate as a contrast mechanism for high-resolution apertureless near-field imaging. Because florescence photons are collected and registered as a function of tip position, specific slices of the optical image may be generated, resulting in high optical contrast. In addition to enhancing the signal-to-noise ratio of the image, this data registration may be used for the 3d reconstruction of optical fields. The resulting tip−sample approach curves were compared to calculations based on the CPS model and were found to be in reasonable agreement with the proposed model. Deeper theoretical understanding of these processes will enable extracting yet additional information such as dipole orientation and QE, all in a single measurement and on time scales common in practical scanning probe microscopy.

Acknowledgment. We dedicate this paper to the memory of Professor Chava Lifshitz, our teacher, colleague, and dear friend. This research was funded in part by the Israel Science Foundation (grant no. 924/04) and by the DIP (German-Israel Program).

Supporting Information Available: Absorption spectrum of the InAs NCs used to functionalize the silicon AFM tip and the emission spectrum of the studied CdSe NCs on the substrate, a schematic of the experimental scheme, and a Flash movie depicting the tip scanning experimental scheme. This material is available free of charge via the Internet at http://pubs.acs.org.

References and Notes

(1) Ambrose, W. P.; Goodwin, P. M.; Martin, J. C.; Keller, R. A. *Science* **1994**, *265*, 364−367.
(2) Xie, X. S.; Dunn, R. C. *Science* **1994**, *265*, 361−364.
(3) Sanchez, E. J.; Novotny, L.; Xie, X. S. *Phys. Rev. Lett.* **1999**, *82*, 4014−4017.
(4) Trabesinger, W.; Kramer, A.; Kreiter, M.; Hecht, B.; Wild, U. P. *Appl. Phys. Lett.* **2002**, *81*, 2118−2120.
(5) Yang, T. J.; Lessard, G. A.; Quake, S. R. *Appl. Phys. Lett.* **2000**, *76*, 378−380.
(6) Lewis, A.; Isaacson, M.; Muray, A.; Harootunian, A. *Biophys. J.* **1983**, *41*, A405.
(7) Dunn, R. C. *Chem. Rev.* **1999**, *99*, 2891.
(8) Zenhausern, F.; Martin, Y.; Wickramasinghe, H. K. *Science* **1995**, *269*, 1083−1085.
(9) Protasenko, V. V.; Gallagher, A.; Nesbitt, D. J. *Opt. Commun.* **2004**, *233*, 45−56.
(10) Krug, J. T.; Sánchez, E. J.; Xie, X. S. *Appl. Phys. Lett.* **2005**, *86*, 233102.
(11) Ebenstein, Y.; Mokari, T.; Banin, U. *J. Phys. Chem. B* **2004**, *108*, 93−99.
(12) Ebenstein, Y.; Mokari, T.; Banin, U. *Appl. Phys. Lett.* **2002**, *80*, 4033−4035.
(13) Jiang, C. Y.; Zhao, J. L.; Therese, H. A.; Friedrich, M.; Mews, A. *J. Phys. Chem. B* **2003**, *107*, 8742−8745.
(14) Gerton, J. M.; Wade, L. A.; Lessard, G. A.; Ma, Z.; Quake, S. R. *Phys. Rev. Lett.* **2004**, *93*, 180801.
(15) Protasenko, V. V.; Gallagher, A. C. *Nano Lett.* **2004**, *4*, 1329−1332.
(16) Becker, H.; Burns, S. E.; Friend, R. H. *Phys. Rev. B* **1997**, *56*, 1893−1905.
(17) Chance, R. R.; Prock, A.; Silbey, R. *Adv. Chem. Phys.* **1978**, *37*, 1−65.
(18) Drexhage, K. H. *J. Lumin.* **1970**, *1−2*, 693.
(19) Kuhn, J. *J. Chem. Phys.* **1970**, *53*, 101.
(20) Tsutsui, T.; Adachi, C.; Saito, S.; Watanabe, M.; Koishi, M. *Chem. Phys. Lett.* **1991**, *182*, 143−146.
(21) Drexhage, K. H. *Prog. Opt.* **1974**, *12*, 165.
(22) Zhang, J.-Y. *Opt. Lett.* **2002**, *27*, 1253−1255.
(23) Protasenko, V. V.; Kuno, M.; Gallagher, A.; Nesbitt, D. J. *Opt. Commun.* **2002**, *210*, 11−23.
(24) Trabesinger, W.; Kramer, A.; Kreiter, M.; Hecht, B.; Wild, U. P. *J. Microsc. (Oxford, U.K.)* **2003**, *209*, 249−253.
(25) Nahum, E.; Ebenstein, Y.; Aharoni, A.; Mokari, T.; Banin, U.; Shimoni, N.; Millo, O. *Nano Lett.* **2004**, *4*, 103−108.
(26) Farahani, J. N.; Pohl, D. W.; Eisler, H. J.; Hecht, B. *Phys. Rev. Lett.* **2005**, *95*, 017402.
(27) Nirmal, M.; Dabbousi, B. O.; Bawendi, M. G.; Macklin, J. J.; Trautman, J. K.; Harris, T. D.; Brus, L. E. *Nature* **1996**, *383*, 802−804.
(28) Stratton, J. *Electromagnetic Theory*; McGraw-Hill: New York, 1941.
(29) Chance, R. R.; Prock, A.; Silbey, R. *J. Chem. Phys.* **1975**, *62*, 2245.
(30) Chung, I. H.; Shimizu, K. T.; Bawendi, M. G. *Proc. Natl. Acad. Sci. U.S.A.* **2003**, *100*, 405−408.
(31) Empedocles, S. A.; Neuhauser, R.; Bawendi, M. G. *Nature* **1999**, *399*, 126−130.
(32) Palik, E. D.; Holm, R. T. *Handbook of Optical Constants of Solids*; Academic Press: New York: 1985.
(33) Tompkins, H. G.; Tasic, S.; Baker, J.; Convey, D. *Surf. Interface Anal.* **2000**, *29*, 179−187.
(34) Brokmann, X.; Coolen, L.; Dahan, M.; Hermier, J. P. *Phys. Rev. Lett.* **2004**, *93*, 107403.
(35) Bohn, J. L.; Nesbitt, D. J.; Gallagher, A. *J. Opt. Soc. Am. A* **2001**, *18*, 2998−3006.
(36) Ordal, M. A.; Long, L. L.; Bell, R. J.; Bell, S. E.; Bell, R. R.; Alexander, R. W., Jr.; Ward, C. A. *Appl. Opt.* **1983**, *22*, 1099−1119.
(37) Grupp, D. E.; Lezec, H. J.; Ebbesen, T. W.; Pellerin, K. M.; Thio, T. *Appl. Phys. Lett.* **2000**, *77*, 1569.
(38) Aeschimann, L.; Akiyama, T.; Staufer, U.; De Rooij, N. F.; Thiery, L.; Eckert, R.; Heinzelmann, H. *J. Microsc.* **2003**, *209*, 182−187.
(39) Buchler, B. C.; Kalkbrenner, T.; Hettich, C.; Sandoghdar, V. *Phys. Rev. Lett.* **2005**, *95*, 063003.